Chemical bonding, interface strength, and oxygen *K* electron-energy-loss near-edge structure of the Cu/Al_2O_3 interface

Teruyasu Mizoguchi,[1,*] Takeo Sasaki,[1] Shingo Tanaka,[2] Katsuyuki Matsunaga,[1,†] Takahisa Yamamoto,[3] Masanori Kohyama,[2] and Yuichi Ikuhara[1]

[1]*Institute of Engineering Innovation, The University of Tokyo, Yayoi, Bunkyo, Tokyo 113-8656, Japan*

[2]*Research Institute for Ubiquitous Energy Devices, National Institute of Advanced Industrial Science and Technology, 1-8-31 Midorigaoka, Ikeda 563-8577, Japan*

[3]*Department of Advanced Materials Science, The University of Tokyo, 5-1-5, Kashiwanoha, Kashiwa, Chiba 277-8561, Japan*

(Received 11 January 2006; revised manuscript received 22 August 2006; published 7 December 2006)

Chemical bondings and oxygen *K* electron-energy-loss near-edge structures (ELNES) of oxygen terminated Cu/Al_2O_3 heterointerfaces with hollow and on-top configurations were theoretically investigated by using a first principles orthogonalized linear combination of atomic orbitals method. From the chemical bonding analysis, it was found that the hollow configuration has stronger ionic and covalent bondings as compared with the on-top configuration, and the weakness of the on-top configuration originates from the strong antibonding interactions between an interfacial oxygen and the second near neighbor Cu. Detailed analysis using overlap population diagrams revealed the formation mechanism of the strong antibonding interactions in the on-top configuration. In the oxygen *K* ELNES calculation, a prepeak feature appears in both configurations and it was predicted that the prepeak for the on-top configuration is larger than that for the hollow configuration. The overlap population diagrams elucidated that the prepeak is mainly composed of the O-Cu antibonding interactions, and the larger prepeak of the on-top configuration originates from the larger O-Cu interactions. The dependence of O-*K* ELNES on the direction of the momentum transfer vector was also discussed. Knowledge of the responsible direction of the momentum transfer vector in relation to the interface orientation was concluded to be indispensable in order to discuss detailed profiles of the ELNES from metal/ceramic heterointerfaces. This study reveals the effect of the atomic configuration of the interface to the chemical bondings, interface strength, and ELNES.

DOI: 10.1103/PhysRevB.74.235408 PACS number(s): 73.20.−r, 73.40.Ns, 79.20.Uv, 82.80.Pv

I. INTRODUCTION

Metal/ceramic heterosystems are used for many kinds of applications, such as solid oxide fuel cells, thermal barrier coatings, electronic packaging devices, and catalysts. Their mechanical and electric properties strongly depend on characters of a junction between the metal and ceramic, i.e., interface. In the vicinity of the interface, misfit dislocations, atomic distortions, charge transfers, and/or different bondings from ordinary compounds are present. An understanding of those peculiar atomic and electronic structures is desirable in order to pave the way to control the properties of the metal and/or ceramic heterosystems. Thus, interface structures of many heterosystems, such as metals on MgO,[1–5] Al_2O_3,[5–22] and YSZ,[23–25] have been studied so far by using high-resolution transmission electron microscopy (HRTEM), electron-energy-loss near-edge structure (ELNES), and/or first principles calculations. Among the metal and/or ceramic systems, Cu/Al_2O_3 is known as a typical metal and/or ceramic heterointerface and studied with experimental and theoretical approaches.[8–22]

Figure 1(a) shows the a typical HRTEM image and O-*K* ELNES of $Cu(111)/Al_2O_3(0001)$ interface which were observed in our previous studies.[10,11] The in-plane orientation relationship of the interface is $[1\bar{1}0]_{Cu}\|[1\bar{1}00]_{Al_2O_3}$, and the terminal plane on the Al_2O_3 side was found to be oxygen.[10,11] A different orientation relationship of $[11\bar{2}]_{Cu}\|[10\bar{1}0]_{Al_2O_3}$ was also observed in the $Cu(111)/Al_2O_3(0001)$ interface by Scheu *et al.*,[20] and they also prepared the Al-terminated interface by an Ar sputtering.[9] In both cases, the interface is categorized as an incoherent interface. Therefore, the interface does not have misfit dislocations and specific periodicities of atomic arrangements. Due to the lack of periodicity, the interface is composed of many kinds of atomic configurations. Two configurations, hollow and on-top, are picked up in Fig. 1(b). The terminated oxygens are situated above the interstitial sites of the interfacial Cu in the hollow configuration, whereas they are located just above the interfacial Cu atoms in the on-top configuration.

So far, effects of the terminal plane, i.e., the stoichiometry, of the interface to the electronic structure and physical strength have been studied by the theoretical calculations.[12,13,15–18] Yang *et al.* compared the electronic structure of the oxygen terminated and Al terminated $Cu(111)/Al_2O_3(0001)$ interfaces, and found that the direction of electron transfer across the interface is opposite to each other for the Al-terminated and oxygen-terminated interfaces.[15] The interface strength is also affected by the kind of terminal plane; the Al-terminated, stoichiometric, interface is commonly concluded to be weaker than the oxygen-terminated, nonstoichiometric, interface.[12,13,15–18]

On the other hand, it was recently elucidated that the local atomic configuration of the interface also plays an important role for the interface strength as well as the kind of terminal plane.[13,17] Tanaka *et al.* calculated the adhesive energy of two kinds of oxygen-terminated $Cu(111)/Al_2O_3(0001)$ interfaces by using the plane-wave basis pseudopotential calculation method, and found that adhesion of the hollow configuration is stronger than that of the on-top configuration.[13] The

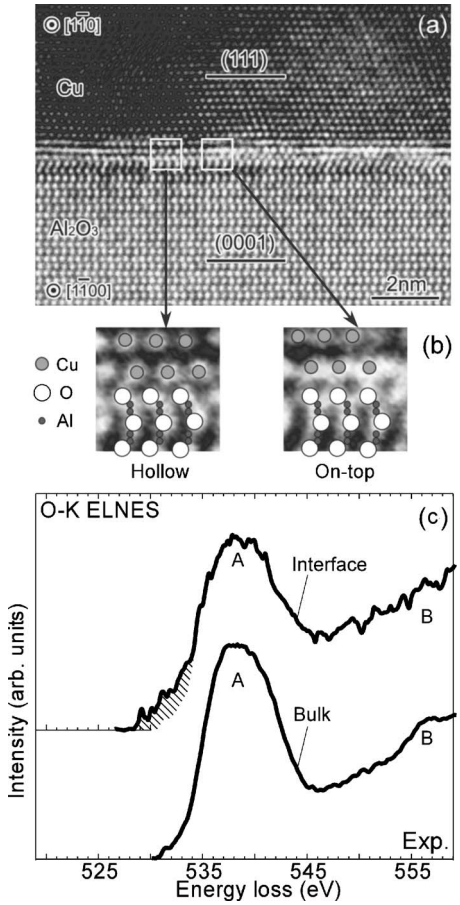

FIG. 1. (a) HRTEM image of Cu(111)/α-Al_2O_3(0001) interface, (b) on-top and hollow configurations at the interface, and (c) experimental O-*K* ELNES from the interface and bulk regions. The ELNES was observed with 2 nm probe. Those HRTEM images and ELNES were reported in Refs. 10 and 11.

same conclusion was also obtained by Hashibon *et al.*[17] They calculated work of separation for several kinds of Cu(111)/Al_2O_3(0001) interfaces with different atomic configurations, terminal planes, and orientation relationships. They also found that the interface strength is changed with the atomic configuration of the interface, and the oxygen terminated interface with the hollow configuration is the most stable interface with respect to cleavage. Similar to the oxygen-terminated interface, they found that the interface strength of the Al-terminated interface is also changed with the atomic configuration of the interface.[17] That is to say, the character of the interfacial oxygen-Cu interaction, which varies with the atomic configuration of the interface, is an important factor for the interface strength. However, most of previous first-principles studies investigated interface energetics (excess interface energies, works of separation, and so on), but the interface adhesion has not been discussed from a viewpoint of chemical bonding theory. This is partly because first-principles plane wave basis calculations commonly used are disadvantageous to obtain an intuitive and quantitative understanding of the chemical bonding states for individual atomic pairs in a system being calculated. In order to reveal a physical and chemical origin of the interface strength, it is desirable to investigate chemical bonds across the interface in a straightforward manner.

In this study, the chemical bondings of two kinds of oxygen-terminated Cu(111)/Al_2O_3(0001) interfaces, the hollow and on-top configurations, were calculated by a first principles orthogonalized linear combination of atomic orbitals method. Since this method can provide detailed chemical bonding states between constituent atoms, the origin of the interface strength and the effect of interfacial atomic-pair configuration is discussed.

In addition, the oxygen-*K* electron-energy-loss near-edge structure (ELNES) from the interface was also calculated because the ELNES has the potential to detect the interfacial oxygen-Cu interactions experimentally. As shown in Fig. 1(c), a prepeak feature, shaded area, has been observed when the spectrum was collected from the interface.[9–11,19,20] Scheu *et al.* performed a multiple scattering calculation of the O-*K* ELNES, and revealed that the prepeak feature originates from the interfacial oxygen-Cu interactions.[9] The ELNES calculation by a first principles band structure method using a sufficiently large supercell was recently performed by the group of the present author,[22] and obtained the same conclusion as Scheu *et al.* However, those studies did not reveal the relationship between the atomic configurations and the prepeak features.

The aim of this study is the elucidation of how the different atomic configurations of the interface affect chemical bondings, interface strength, and ELNES.

II. ATOMIC STRUCTURE AND COMPUTATIONAL PROCEDURE

The lattice mismatch between α-Al_2O_3 (0001) and fcc-Cu (111), approximately 7%, was compensated by expanding the Cu slab to the parallel direction of the interface plane (IP). The atomic structures of the constructed interfaces were optimized by using a first principles plane-wave pseudopotential method in our previous study.[13] In the optimization calculations, norm-conserving pseudopotentials were used with as plane-wave cutoff energy of 70 Ry. The structure optimization was performed by using the 33-atom supercells, which contains an Al_2O_3 (0001) slab with four O and six Al layers sandwiched by two Cu slabs with five (111) layers. Four sampling *k* points were in the irreducible sixth of the hexagonal Brillouine zone. The details of the pseudopotential calculations were described elsewhere.[13]

In this study, the supercells were repeated by $2\times2\times1$, and the 132-atom supercells, $a=b=9.42$ Å and $c=17.78$ Å for the on-top configuration and 16.89 Å for the hollow configuration, were used in order to calculate ELNES correctly. The chemical bondings and ELNES calculations were performed by using an orthogonalized linear combination of atomic orbitals (OLCAO) method within a local-density approximation (LDA) of the density-functional theory (DFT).[26] The most important advantage of this method is that the chemical bonding can be calculated directly because the wave functions are given by linear combinations of the atomic orbitals. In addition, the core orbitals are eliminated from the final secular equation by an orthogonalized process

TABLE I. Used basis functions in this study.

	Cu	Al	O
Core:	[Ar]	[Ne]	[He]
Minimal:	$4s,4p,3d,4d$	$3s,3p,3d$	$2s,2p$
Full:	$4s,5s,4p,5p,3d,4d$	$3s,4s,3p,4p,3d$	$2s,3s,2p,3p$
Extended:	$4s,5s,6s,4p,5p,6p,3d,4d,5d$	$3s,4s,5s,3p,4p,5p,3d,4d$	$2s,3s,4s,2p,3p,4p$

in the OLCAO method. This can significantly reduce the computational time and is very effective to calculate a large and complicated system, such as grain boundaries and interfaces.[27–30]

The overlap population between orbitals i and j at the nth band is defined as follows in the Mulliken scheme:[31]

$$q_{i,j}^{n} = A_i^{n^*} A_j^n S_{i,j}. \tag{1}$$

A_i^n is the eigenvector component of the ith orbital in the nth orbital in the nth band, and $S_{i,j}$ is the overlap integral. A bond overlap population (BOP) of a pair of atoms (a and b), $Q_{a,b}$, and effective charge of an atom a, Q_a^*, is given by the following equation:

$$Q_{a,b} = \sum_{n,occ} \sum_{i\in a} \sum_{j\in b} q_{i,j}^n, \quad Q_a^* = \sum_{n,occ} \sum_{i\in a} \sum_{j} q_{i,j}^n \tag{2}$$

Subtraction of Q_a^* from the atomic number Z provides the net charge (NC), ΔQ_a^*. The magnitude of the ionicity and covalency can be represented by using ΔQ_a^* and $Q_{a,b}$, respectively.

The theoretical spectrum of ELNES is obtained by calculating the electron dipole transition probability (I) from a core orbital to the unoccupied bands:

$$I \propto \sum_f |\langle f|\mathbf{E}\cdot\mathbf{r}|i\rangle|^2 \delta(\hbar\omega - E_f + E_i). \tag{3}$$

f and i are one electron wave functions at the final and initial states. $\hbar\omega$, E_f, and E_i are a transition energy and a total energy of the supercell at the final and initial states, respectively. $\mathbf{r}$ is a position operator of an electron $\mathbf{E}$ is a momentum transfer vector of a scattered electron. Both the final and ground states were separately calculated, and the theoretical transition energy of ELNES was evaluated by the total energy difference between the ground state and the final state. In order to compare with the experimental spectra, each transition probability is broadened by using the Gaussian function of $\Gamma = 2.0$ eV, which was determined so as to obtain the best reproduction of the experimental O-K ELNES of Al_2O_3. Details of the ELNES calculation were reported elsewhere.[32–34]

Table I shows basis function sets used in this study. In the self-consistent iteration for a stable electronic structure, the full basis function set was employed. After calculation of the stable electronic structure, separate calculations using the minimal and extended basis sets for the Mulliken population analysis and the ELNES calculations, respectively.

Since four k points for the 33-atom supercells were used in the pseudopotentical calculation,[13] one k point in the irreducible portion of the Brillouin zone for the 133-atoms supercell was used for self-consistent iterations in the OLCAO calculation. The convergence of total energy with respect to the number of k point was confirmed to be 0.17 meV/atom by calculating the hollow model with two general k points. Eight k points and twenty-seven k points were used for the ELNES calculation and the Mulliken population analysis, respectively.

III. RESULTS AND DISCUSSION

A. Chemical bondings of Cu/Al_2O_3 interface

Figure 2 shows atomic structures in the vicinity of the interfaces. The first and second Cu layers are called "Cu 1st" and "Cu 2nd." An interfacial oxygen, the first and second near neighbor Cu and Al are called "O", "Cu_1", "Cu_2", "Al_1", and "Al_2", respectively. The subscripts "h" and "o" are used when it is necessary to distinguish atoms in the hollow and on-top configurations. Bond lengths, lattice constants of the supercells, and interlayer distances are also summarized in the same figure.

Density of states (DOS) and partial DOS (PDOS) were shown in Fig. 3 together with those of α-Al_2O_3 and Cu metal. "s", "p", and "d", respectively, represents the sum of s-type, p-type, and d-type orbitals. In both interface models, it is commonly found that oxygen-s bands form semicore states around −18 eV and the valence bands are composed of oxygen-p, Cu-s, Cu-p, and Cu-d bands. As compared with α-Al_2O_3, the oxygen p-PDOS at the energy range from 0 to −3 eV is smaller in the hollow configuration, whereas larger in the on-top configuration. Regarding Cu-d bands, the position of the Cu-d band of Cu 2nd is close to that of the Cu metal, whereas it shifts to the higher energy side at Cu 1st, about 1 eV in the hollow configuration and 0.3 eV in the on-top configuration. Those differences from the bulk compounds are caused by the presence of the heterointerface, and that between the interface models is ascribed to the different atomic configuration of the interface. In order to discuss electronic structures quantitatively, net charges (NC) and bond overlap populations (BOP) are discussed below.

The NC and BOP are summarized in Table II. The NC of Cu_{h1} and Cu_{o1} are +0.43 and +0.32, respectively. The positive NC indicates the electron transfer from Cu to oxygen across the interfaces. This is consistent to the result obtained by Yang *et al.*[15] In both configurations, it is commonly found that the Cu 2nd exhibits slightly positive NC, and the NC of Al_1 are smaller than that of Al_2. Regarding the BOP, O-Al_1

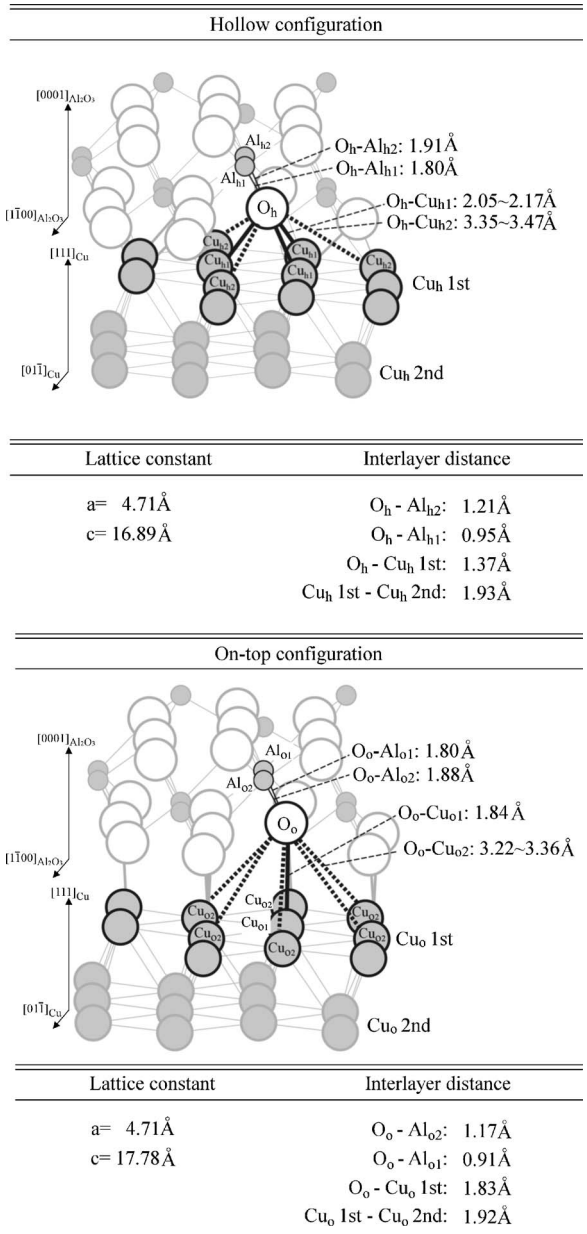

FIG. 2. Atomic structure in the vicinity of the interfaces. The atomic structure was optimized by a first principles pseudopotential method (Ref. 13).

exhibits higher BOP than O-Al$_2$. This results in the lower NC of the Al$_1$ than the Al$_2$. It should be mentioned that O$_o$-Cu$_{o1}$ has approximately five times larger BOP than O$_h$-Cu$_{h1}$, and BOP of O$_h$-Cu$_{h2}$ and O$_o$-Cu$_{o2}$ are negative. The negative BOP indicates that the bond is composed of out-of-phase interactions, i.e., antibonding interactions. It is also found that not only O-Cu$_1$ bonding interactions but also the O-Cu$_2$ antibonding interactions are higher in the on-top configuration than that in the hollow configuration.

Although the magnitude of the O-Cu$_2$ antibonding interaction is much smaller than that of the O-Cu$_1$ bonding interaction in both configurations, the contribution of the O-Cu$_2$ antibonding interaction to the interface strength should be important when the number of the bond is large. In the hollow configuration, the number of O$_h$-Cu$_{h1}$ is identical to that of O$_h$-Cu$_{h2}$, and thus the total antibonding interaction for one interfacial oxygen becomes −0.09, which is less than one-fourth of the total bonding interaction, 0.39 (see Table II). On the contrary, the number of the O$_o$-Cu$_{o2}$ is six times of the O$_o$-Cu$_{o1}$, though the absolute value of the antibonding interaction of O$_o$-Cu$_{o2}$ is one-seventh of the bonding interaction of O$_o$-Cu$_{o1}$ (see Table II). By accounting for the number of the bonds at the interface, the total antibonding interaction of O$_o$-Cu$_{o2}$ becomes −0.48, which is close to the total bonding interaction of O$_o$-Cu$_{o1}$, +0.59 (see Table II).

In order to discuss the interface strength, the strength of the ionic bonding at the interface (σ_{Ionic}) is evaluated by the Coulomb interaction between the interfacial oxygen and Cu layers of a unit area (A), which is defined as follows:

$$\sigma_{Ionic} = \left(\frac{\sum_{Interfacial} \Delta Q^*_{oxygen} \times \sum_{Interfacial} \Delta Q^*_{\mathrm{Cu}}}{r} \right) \Big/ A, \tag{4}$$

in which r is the interlayer distance of the interface.

The strength of the covalent bonding of the interface ($\sigma_{Covalent}$) is obtained by the following equation:

$$\sigma_{Covalent} = \left(\sum_{Interfacial} Q_{oxygen,\mathrm{Cu}} \right) \Big/ A. \tag{5}$$

$\sigma_{Covalent}$ contains not only the first nearest neighbor but also the second and further Cu-O interactions. $\sigma_{Covalent}$ is plotted with σ_{Ionic} in Fig. 4. It is clearly seen that the hollow configuration has the stronger ionic and covalent bondings. Namely, the hollow configuration can be concluded to be stronger than the on-top configuration. The conclusion is consistent with the previous reports.[13,14,17] Here, it should be mentioned again that the O$_o$-Cu$_{o2}$ antibonding interaction is as strong as the O$_o$-Cu$_{o1}$ bonding interaction, while the antibonding interaction in the hollow interface model is almost negligible. That is to say, the weakness of the on-top configuration is ascribed to the strong O$_o$-Cu$_{o2}$ antibondings. The reason why the antibonding interaction is large in the on-top configuration is discussed below by using overlap population (OP) diagrams.

The OP diagram was originally proposed as crystal orbital overlap population (COOP) diagrams by Hoffmann[35] OP diagram can be obtained by plotting the overlap population ($q_{a,b}$) between a pair of atoms at each band, and can visually show orbital-orbital interactions. The OP diagram has been employed to understand electronic structures and interpret ELNES.[36–38] The OP diagrams of O-Cu$_2$, O-Cu$_1$, and O-O are displayed in Fig. 5. Since the valence band is mainly composed of O-p bands, the interactions with O-p bands were calculated. Characteristic differences can be found at the top of the valence band, which are indicated by arrows in Fig. 5(d). The magnitude of the O-Cu$_1$ bonding, O-Cu$_2$ antibonding, and O-O antibonding interactions are apparently higher in the on-top configuration. In addition, they appear at the same band. The large O-Cu$_{o1}$ bonding and O-Cu$_{o2}$ antibonding interactions are the origins of the large O-Cu$_{o1}$ BOP (see Table II) and the weakness of the on-top configuration, respectively. On the other hand, anion-anion antibonding is

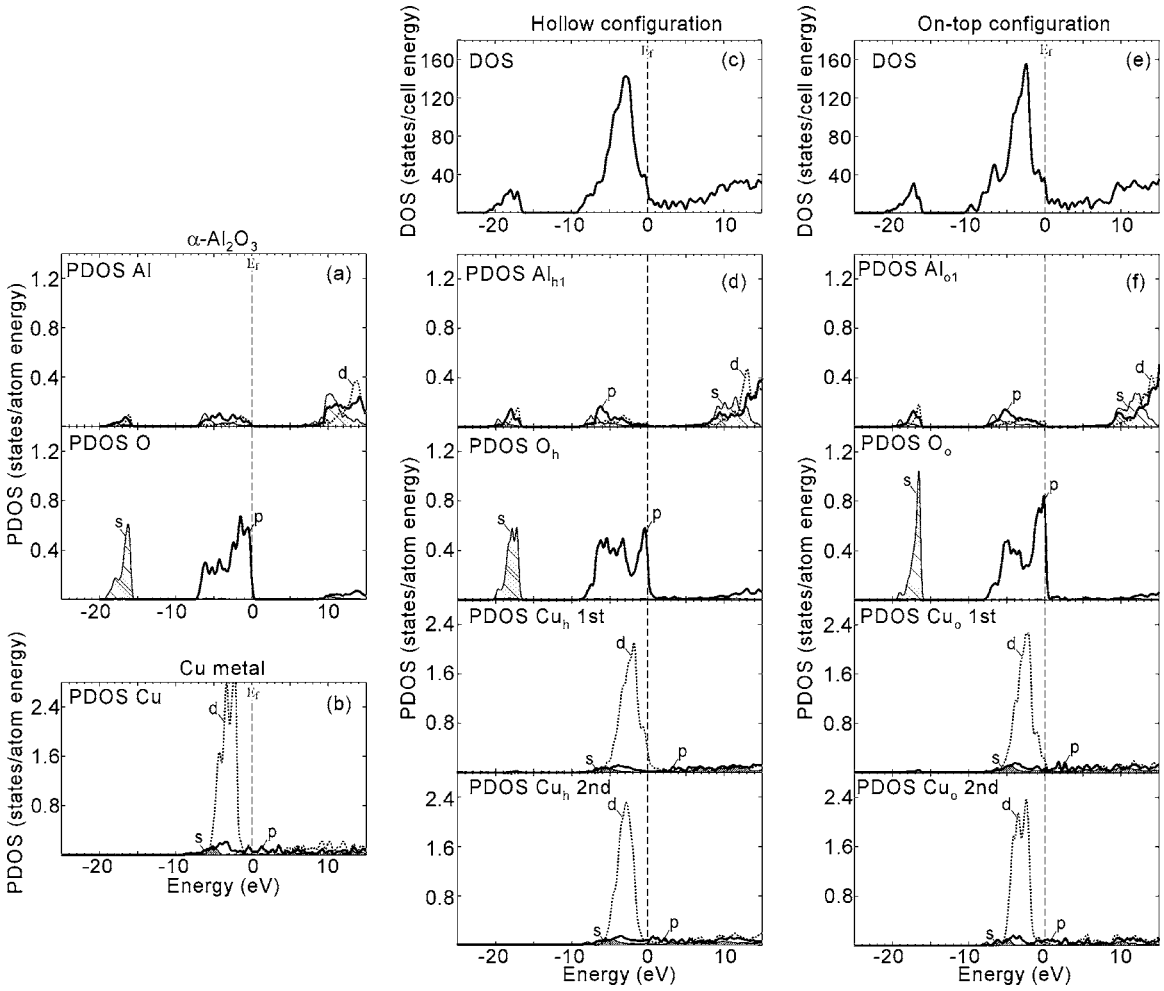

FIG. 3. (a, b) PDOS for α-Al_2O_3 and Cu metal and (c, d) DOS and PDOS for the hollow configuration and (e, f) the on-top configuration. The DOS calculations were separately performed using a minimal basis function set. Thin dashed lines represent the position of the top of the valence band.

usually formed at the top of the anion band,[36] and it appears at the top of the valence band in the case of Cu/Al_2O_3. The similar but weaker O-O antibonding interaction is found in the hollow configuration [Fig. 5(b)]. By taking into account those points, the formation mechanism of the strong O_o-Cu_{o2} antibonding interactions is understood as follows:

Here, let us take four atoms at the on-top configuration, $Cu_{o(1)}$, $Cu_{o(2)}$, $O_{o(1)}$, and $O_{o(2)}$ [Fig. 6(a)]. For simplicity, the wave functions are schematically drawn by circle. The phase of the wave function, + and −, is represented by white and gray, and the solid and dashed belts represent the bonding

TABLE II. Calculated net charges and bond overlap populations.

Hollow configuration		On-top configuration	
	Net Charge		
Al_{h2}	+0.68	Al_{o2}	+0.73
Al_{h1}	+0.26	Al_{o1}	+0.42
O_h	−0.53	O_o	−0.61
Cu_h 1st	+0.43	Cu_o 1st	+0.32
Cu_h 2nd	+0.14	Cu_o 2nd	+0.13
	Bond overlap population (number of bond)		
O_h-Al_{h2}	0.59 (1)	O_o-Al_{o2}	0.64 (1)
O_h-Al_{h1}	0.83 (1)	O_o-Al_{o1}	0.80 (1)
O_h-Cu_{h1}	0.13 (3)	O_o-Cu_{o1}	0.59 (1)
O_h-Cu_{h2}	−0.03 (3)	O_o-Cu_{o2}	−0.08 (6)

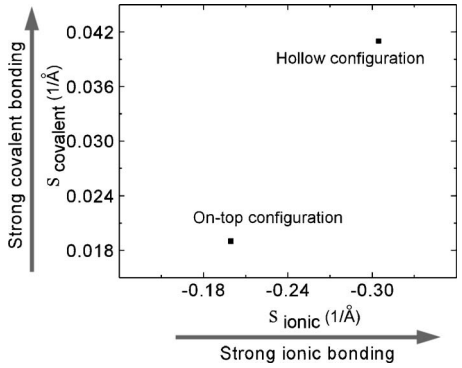

FIG. 4. Covalent bonding strength ($\sigma_{covalent}$) is plotted with ionic bonding strength (σ_{ionic}) of the interfaces.

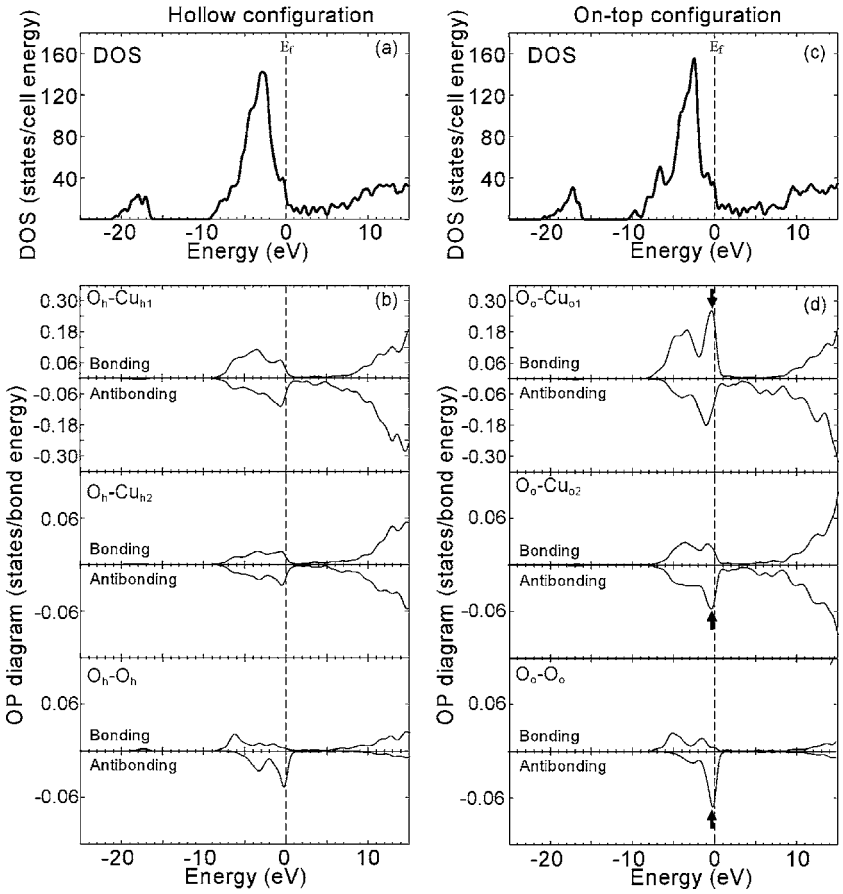

FIG. 5. (a, b) DOS and overlap population (OP) diagrams for the hollow configuration and (c, d) the on-top configuration.

and antibonding interactions. The $Cu_{o(1)}$ and $Cu_{o(2)}$ make bonding interactions with the respective on-top oxygens, $O_{o(1)}$ and $O_{o(2)}$. Then, the phases of the wave functions of $Cu_{o(1)}$ and $Cu_{o(2)}$ are the same as those of $O_{o(1)}$ and $O_{o(2)}$, respectively. On the other hand, the phase of the wave function of $O_{o(1)}$ is needed to be different from that of $O_{o(2)}$ in order to form the $O_{o(1)}$-$O_{o(2)}$ antibonding interaction. When the $O_{o(1)}$-$Cu_{o(1)}$ bonding, $O_{o(2)}$-$Cu_{o(2)}$ bonding, and $O_{o(1)}$-$O_{o(2)}$ antibonding interactions are formed at the same time, the phase of the wave functions of $Cu_{o(1)}$ and $Cu_{o(2)}$ is different from that of $O_{o(2)}$ and $O_{o(1)}$, respectively, and then the $O_{o(1)}$-$Cu_{o(2)}$ and $O_{o(2)}$-$Cu_{o(1)}$ become antibonding.

The wave functions at the top of the valence band of the Γ point are shown below the schematic illustration [Fig. 6(b)]. They were obtained on the interfacial Cu_1-O-Cu_2 planes. Similar to the schematic illustration, the formation of the $O_{o(1)}$-$Cu_{o(1)}$, $O_{o(2)}$-$Cu_{o(2)}$ bonding, $O_{o(1)}$-$O_{o(2)}$ antibonding, and $O_{o(1)}$-$Cu_{o(2)}$, $O_{o(2)}$-$Cu_{o(1)}$ antibondings is clearly seen. On the contrary, it is found that the individual bonding and antibonding interactions in the hollow configuration is relatively weaker than that in the on-top configuration [Fig. 6(c)]. Although the bonding interaction of the O_h-Cu_{h1} is much weaker than that of the O_o-Cu_{o1} (Table II), the larger number of the moderate bonding interactions and the smaller number of the weaker antibonding interactions make "better" balance in the hollow configuration and result in the stronger interface (see Table II and Fig. 4).

B. Electron energy loss near edge structures of Cu/Al_2O_3 interfaces

As described above, the ELNES has the potential to detect the interfacial O-Cu interactions experimentally. Especially, recent progress of a scanning TEM (STEM) equipments enables us to observe ELNES in an atomic resolution. On the other hand, a theoretical calculation is indispensable to interpret ELNES. For the ELNES calculation, it has been known that the introduction of a core hole, which is generated at the core orbital in an electron transition process, is essential.[37] In addition, a sufficiently large supercell is necessary to minimize interactions among the core-holed atoms in adjacent cells.[32–34,38] Therefore, one hundred thirty two atom supercells were used in this study and one core hole was rigorously included at the O-1*s* core orbital.

Figure 7 shows the experimental and calculated O-*K* ELNES. The experimental spectra were observed in our previous study,[10,11] and the calculated spectra from the first and second near neighbor oxygens to the interfaces were separately obtained by introducing the core hole at the respective oxygen. Although the onsets of the calculated spectra were shifted by +6 eV, it should be noted that the calculation error is less than 1.2% of the absolute transition energy. Calculated O-*K* ELNES of α-Al_2O_3 is superimposed on that of the first nearest neighbor oxygen. As compared with α-Al_2O_3, it is found that peak *A* is broader and peaks *A* and *B* slightly shift to the higher energy side in both interface models. A characteristic feature for the interfacial oxygens can be found at the

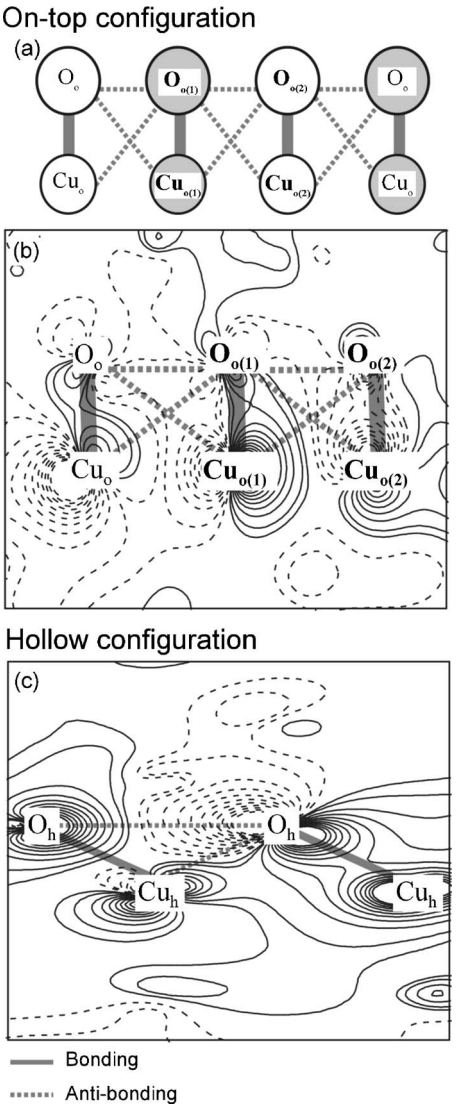

FIG. 6. (a) Schematic illustration of the formation mechanism of the antibonding interaction in the on-top configuration. Four atoms are named $Cu_{o(1)}$, $Cu_{o(2)}$, $O_{o(1)}$, and $O_{o(2)}$. For simplicity, wave functions are represented by circles. White and gray represent the phase of the wave functions, + and −. Solid and dashed belts are used to represent bonding and antibonding interactions, respectively. (b, c) Wave functions of the on-top and hollow configurations at the top of the valence band of the Γ point on the Cu_1-O-Cu_2 planes. Solid and dashed contour lines represent plus and minus phase of the wave function, respectively. The contour lines are from 0.10 to −0.10 in intervals of 0.01.

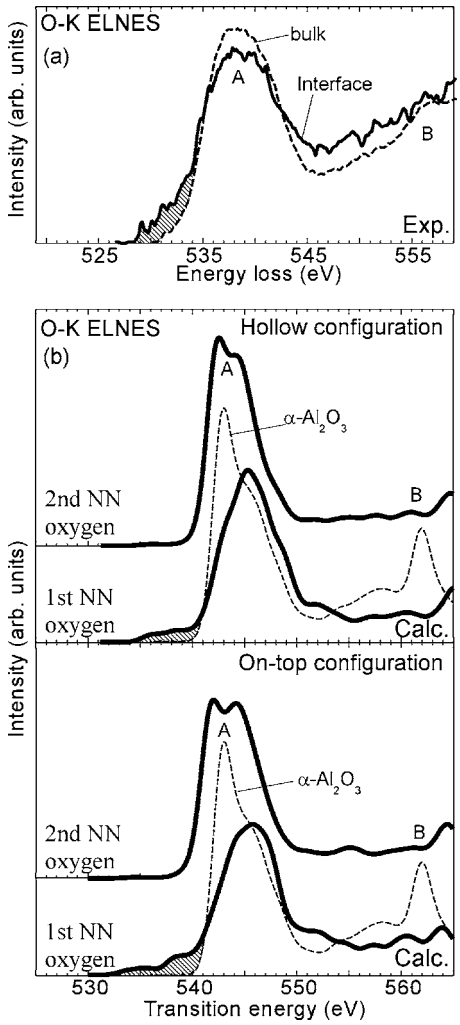

FIG. 7. (a) Experimental (Refs. 10 and 11) and (b) calculated O-*K* ELNES. The first and second near neighbor (NN) oxygens were separately calculated. O-*K* ELNES from the bulk α-Al_2O_3 area and the calculated O-*K* ELNES of α-Al_2O_3 are superimposed with dashed lines.

front of peak *A*, i.e., prepeak. They were shaded in the figure. By comparing the size of the shaded area, it was found that the prepeak for the on-top configuration is 57% larger than that for the hollow configuration. At the second near neighbor oxygen sites, it is found that the prepeak intensity remarkably decreases. This indicates that the prepeak mainly originates from the interfacial O-Cu interactions.

In order to interpret the calculated spectra, the OP diagrams of the conduction bands at the final state were computed. Although the in-phase and the out-of-phase interactions correspond to "bonding" and "antibonding" only when the bands are occupied, the same phrases are applied to the unoccupied bands for simplicity. Figure 8 shows the OP diagrams of O-Cu_1, O-Cu_2, and O-Al_1. In order to focus the prepeak, the energy region between the prepeak and peak *A* is magnified. It is found that peak *A* and prepeak mainly originates from the O-Al and the O-Cu antibonding interactions, respectively. Both bonding and antibonding interactions at the prepeak area of the on-top configuration are 50–78% larger than that of the hollow configuration. Therefore, the larger prepeak in the on-top configuration is ascribed to the larger O-Cu interactions, including bonding and antibonding.

Regarding the relationship between the prepeak and the interface strength, it is concluded that the integrated prepeak intensity is not proportional to the interface strength even though the prepeak is mainly caused by the interfacial O-Cu interactions. The integrated prepeak intensity is higher in the on-top interface, whereas the on-top interface is weaker than the hollow interface. As discussed above, larger interactions, including both bonding and antibonding interactions, cause

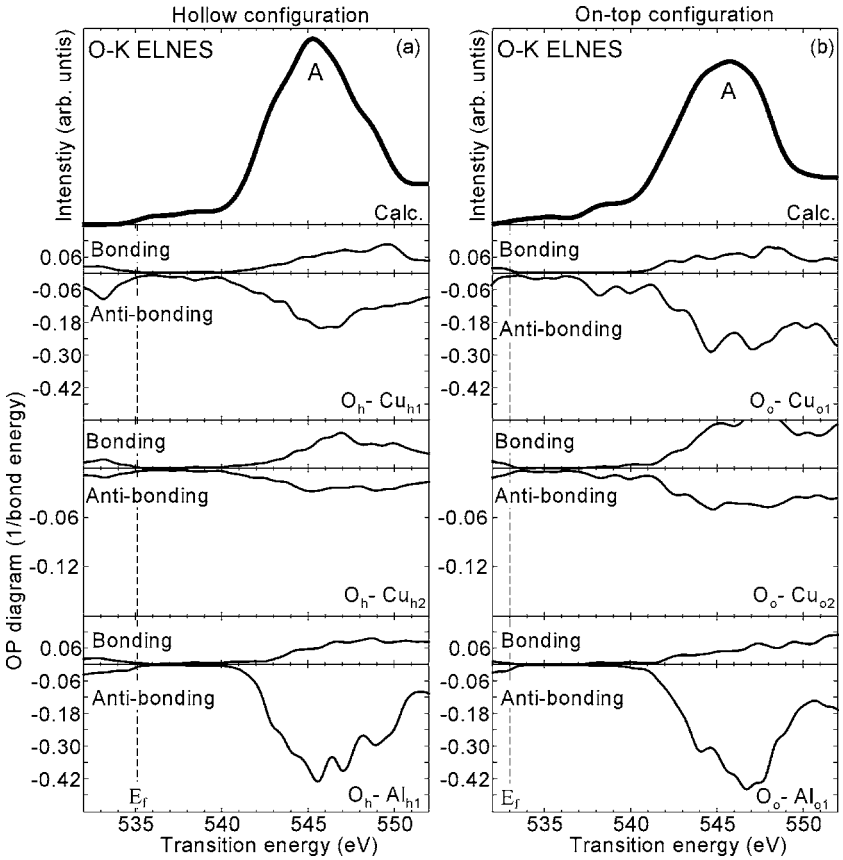

FIG. 8. Calculated O-*K* ELNES and OP diagrams of (a) the hollow configuration and (b) the on-top configuration. The OP diagrams were obtained at the O-1*s* core holed state. Thin dashed lines represent the position of the top of the valence band.

the larger prepeak of the on-top configuration, whereas the stronger and larger number of the antibonding interactions makes the on-top configuration weaker.

Recently, the O-*K* ELNES from a $Cu(001)/Al_2O_3(11\bar{2}0)$ interface was observed by the group of the present authors, and found that the prepeak is apparently larger than that from the $Cu(111)/Al_2O_3(0001)$ interface.[11,21] Although the calculation of the interface has not been performed due to the difficulty to construct the interface model, it is expected that the magnitude of the Cu-O interactions is larger than that in the $Cu(111)/Al_2O_3(0001)$ interface. In fact, the interface distance for the $Cu(001)/Al_2O_3(11\bar{2}0)$ interface is shorter than that for the $Cu(111)/Al_2O_3(0001)$ interface.[11,21] However, as we mentioned above, it does not imply that the $Cu(001)/Al_2O_3(11\bar{2}0)$ interface is mechanically stronger than the $Cu(111)/Al_2O_3(0001)$ interface. Within the authors' best knowledge, the interface strength of the $Cu(001)/Al_2O_3(11\bar{2}0)$ interface have not been reported so far.

C. Dependence of O-*K* ELNES on the direction of the momentum transfer vector

The spectral feature of ELNES changes with the direction of the momentum transfer vector when a probed area is crystallographically anisotropic.[39–46] Since the interface is a kind of two-dimensional structure, the electronic structures along the perpendicular direction to the interface plane (IP) is different from that along the parallel direction. Here, we discuss the dependence of the O-*K* ELNES on the direction of the momentum transfer vector of the scattered electron.

Equation (3) can be rewritten by the electron dipole transition to each possible direction, *x*, *y*, and *z* as follows:

$$I \propto \sum_f [|\langle f_x|\mathbf{E}_x \cdot \mathbf{r}_x|i_x\rangle|^2 + |\langle f_y|\mathbf{E}_y \cdot \mathbf{r}_y|i_y\rangle|^2 + |\langle f_z|\mathbf{E}_z \cdot \mathbf{r}_z|i_z\rangle|^2 + \mathbf{A}^2]\delta(\hbar\omega - E_f + E_i). \quad (6)$$

A is a cross term among *x*, *y*, and *z* directions.[41] The directional dependence can be theoretically simulated by calculating the corresponding term in the square bracket of the above equation. In case of this study, the IP is placed on the *xy* plane and the directions parallel and perpendicular to the IP are focused. Figure 9 shows the calculated spectrum with the different direction of the momentum transfer vector. Although the dependence is relatively small in the case of α-Al_2O_3, the spectra from the interfaces are apparently changed by the direction of the momentum transfer vector. On the other hand, the magnitude of the directional dependence becomes smaller at the second near neighbor oxygen and tends to be similar to that of α-Al_2O_3.

It should be mentioned that the prepeak almost disappears when the momentum transfer vector is parallel to the IP. Thus, it is concluded that the prepeak feature mainly originates from the unidirectional O-Cu interactions across the interface. In addition, it is found that the magnitude of the directional dependence seems to be larger in the on-top configuration. This is ascribed to the well-oriented O-Cu_1 interactions in the on-top configuration: The O_o-Cu_{o1} is perpendicular to the IP, whereas the unidirectionality is relatively

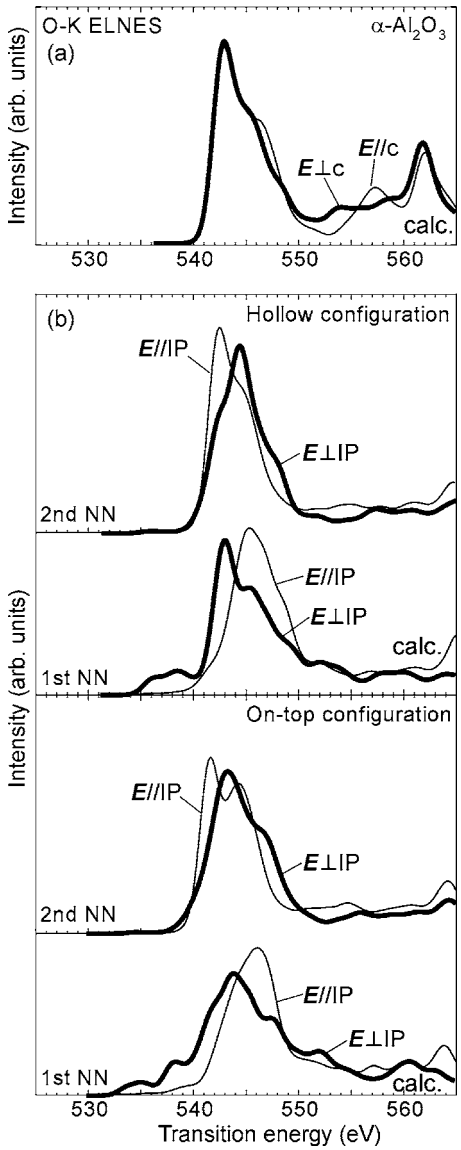

FIG. 9. (a) The dependence on the direction of the momentum transfer vector of O-*K* ELNES of α-Al_2O_3, (b) the hollow configuration, and the on-top configurations. "**E**" represents the direction of the momentum transfer vector of the scattered electron. Parallel and perpendicular directions to the interface plane (IP) are shown.

broken in the hollow configuration, this is also confirmed by the wave-function plots shown in Fig. 6. Although the dependence of the momentum transfer vector on O-*K* ELNES from the interface has not been reported so far, this calculation predicts that the prepeak feature becomes larger when the direction of the momentum transfer vector is perpendicular to the IP, whereas the change of the direction to the parallel to the IP makes the prepeak feature smaller.

The direction of the momentum transfer vector of the scattered electron is changed by not only the crystallographic orientation of the specimen but also the incidence angle, scattered angle, collection angle, and some lens conditions of the instruments.[39–46] This result clearly indicates that the responsible direction of the momentum transfer vector for the observed ELNES is an indispensable information in order to discuss the fine profiles of the ELNES from the metal/ceramic interface.

IV. CONCLUSIONS

We investigated the chemical bonding, interface strength, and O-*K* ELNES of the Cu/Al_2O_3 interfaces by using the first principles orthogonalized linear combination of atomic orbitals method. The main results in this study are summarized as follows:

(1) Cu atoms in Cu 1st and Cu 2nd layer exhibit positive net charge and the net charge of Al_1 is smaller than that of Al_2. This indicates that the electron transfer takes place from Cu to α-Al_2O_3 by the presence of the heterointerface.

(2) The O_o-Cu_{o1} and O_h-Cu_{h1} are made by the bonding interactions, whereas the O_h-Cu_{h2} and O_o-Cu_{o2} are composed of the antibonding interactions. The contribution of the antibonding to the interface strength of the hollow configuration was concluded to be negligible, whereas it was found that the antibonding interaction plays an important role in the on-top configuration.

(3) The interface strength was discussed by using the net charge and bond overlap population, and found that the hollow configuration has stronger ionic and covalent bondings than the on-top configuration. The origin of the weakness of the on-top configuration is ascribed to the stronger and larger number of O_o-Cu_{o2} antibonding interactions. By using overlap population diagrams, the formation mechanism of the strong antibonding interaction in the on-top configuration was elucidated.

(4) O-*K* ELNES from the interfaces were calculated. The prepeak feature appears in both configurations, and it was predicted that the on-top configuration has a larger prepeak. The overlap population diagrams revealed that the prepeak is mainly formed by antibonding interactions among the interfacial oxygen and the neighboring Cu. It was also found that both bonding and antibonding are stronger in the on-top configuration. It was concluded that the stronger O-Cu interactions contribute to the larger prepeak of the on-top configuration, and the integrated prepeak intensity is not proportional to the interface strength even though the prepeak is mainly caused by the interfacial O-Cu interactions.

(5) The dependence of the O-*K* ELNES on the direction of the momentum transfer vector of the scattered electron was discussed. It was predicted that ELNES apparently change in relation to the direction of the interface plane. The prepeak almost disappears when the momentum transfer vector is parallel to the interface plane. The detail knowledge of the responsible direction for the observed ELNES was concluded to be indispensable in order to discuss the fine profiles of the ELNES from the metal and/or ceramic interface.

Last, we focused the relationship among the atomic and electronic structures and ELNES of a metal/ceramic interface. It has been often claimed that the ELNES, as well as x-ray absorption spectrum, has a potential to provide information on atomic and electronic structures and chemical bondings. However, we would emphasize that the connection between the ELNES profiles and those desirable information is not always direct or proportional because the conduction

band, which is responsible for ELNES, is not identical to the valence band. Especially, the relationship between the ELNES and physical properties is ambiguous so far. In the case of Cu/Al_2O_3 interface, the integrated intensity of the prepeak is not proportional to the interface strength even though it purely originates from the interfacial O-Cu interactions.

The only way to find an intersection between ELNES and physical properties are detailed investigations of the electronic structures. We believe that this paper well demonstrated it and provided the relationships among chemical bondings, properties, and ELNES.

ACKNOWLEDGMENTS

We thank W. Y. Ching at the University of Missouri-Kansas City for allowing us to use the OLCAO code. T.S. is financially supported by the Japan Society for Promotion of Science (JSPS). This work is supported by a Grant-in-Aid for General Scientific Research from the Ministry of Education, Sports, Science and Culture of Japan and partially supported by the New Energy and Industrial Technology Development Organization (NEDO), Japan, The Murta Science Foundation, and Iketani Science and Technology Foundation.

*Corresponding author. Email address: mizoguchi@sigma.t.u-tokyo.ac.jp

†Present address: Department of Materials Science & Engineering, Kyoto University, Yoshida, Sakyo, Kyoto 606-8501, Japan.

[1] M. W. Finnis, J. Phys.: Condens. Matter **8**, 5811 (1996).
[2] Y. Ikuhara, P. Pirouz, S. Yadavalli, and C. P. Flynn, Philos. Mag. A **72**, 179 (1995).
[3] C. Li, R. Wu, A. J. Freeman, and C. L. Fu, Phys. Rev. B **48**, 8317 (1993).
[4] I. Tanaka, M. Mizuno, S. Nakajo, and H. Adachi, Acta Mater. **46**, 6511 (1998).
[5] Y. Ikuhara and P. Pirouz, Microsc. Res. Tech. **40**, 206 (1998).
[6] Y. Ikuhara, P. Pirouz, A. H. Heuer, S. Yadavalli, and C. P. Flynn, Philos. Mag. A **70**, 75 (1994).
[7] J. Bruly, R. Brydson, H. Müllejans, J. Mayer, G. Gutekunst, W. Mader, D. Knauss, and M. Rühle, J. Mater. Res. **9**, 2574 (1994).
[8] G. Dehm, M. Rühle, G. Ding, and R. Raj, Philos. Mag. B **71**, 1111 (1995).
[9] C. Scheu, G. Dehm, M. Rühle, and R. Brydson, Philos. Mag. A **78**, 439 (1998).
[10] T. Sasaki, K. Matsunaga, H. Ohta, H. Hosono, T. Yamamoto, and Y. Ikuhara, Sci. Technol. Adv. Mater. **4**, 575 (2003).
[11] T. Sasaki, T. Mizoguchi, K. Matsunaga, S. Tanaka, T. Yamamoto, M. Kohyama, and Y. Ikuhara, Appl. Surf. Sci. **241**, 87 (2005).
[12] W. Zhang, J. R. Smith, and A. G. Evans, Acta Mater. **50**, 3803 (2002).
[13] S. Tanaka, R. Yang, M. Kohyama, T. Sasaki, K. Matsunaga, and Y. Ikuhara, Mater. Trans. **45**, 1973 (2004).
[14] S. Tanaka, R. Yang, and M. Kohyama, (unpublished).
[15] R. Yang, S. Tanaka, and M. Kohyama, Philos. Mag. Lett. **84**, 425 (2004).
[16] R. Yang, S. Tanaka, and M. Kohyama, Philos. Mag. **85**, 2961 (2005).
[17] A. Hashibon, C. Elsässer, and M. Rühle, Acta Mater. **53**, 5323 (2005).
[18] M. Kohyama, S. Tanaka, K. Okazaki, R. Yang, and Y. Morikawa, Mater. Sci. Forum **502**, 27 (2005).
[19] S. V. Dmitriev, N. Yoshikawa, M. Kohyama, S. Tanaka, R. Yang, and Y. Kagawa, Acta Mater. **52**, 1959 (2004).
[20] C. Scheu, S. H. Oh, T. Wagner, and M. Rühle, Microsc. Microanal. **9**, 298 (2003).
[21] T. Sasaki, T. Mizoguchi, K. Matsunaga, S. Tanaka, T. Yamamoto, M. Kohayma, and Y. Ikuhara, Mater. Sci. Forum **475**, 3859 (2005).
[22] T. Sasaki, T. Mizoguchi, K. Matsunaga, S. Tanaka, T. Yamamoto, M. Kohyama, and Y. Ikuhara, J. Jpn. Inst. Met. **69**, 86 (2005).
[23] X. Han, Y. Zhang, and H. Xu, Chem. Phys. Lett. **378**, 5816 (2001).
[24] J. I. Beltrán, S. Gallego, J. Cerdá, J. S. Moya, and M. C. Muñoz, Phys. Rev. B **68**, 075401 (2003).
[25] T. Sasaki, K. Matsunaga, H. Ohta, H. Hosono, T. Yamamoto, and Y. Ikuhara, Mater. Trans. **45**, 2137 (2004).
[26] W. Y. Ching, J. Am. Ceram. Soc. **73**, 3135 (1990).
[27] P. Rulis, W. Y. Ching, and M. Kohyama, Acta Mater. **52**, 3009 (2004).
[28] J. Chen, Y. N. Xu, P. Rulis, L. Ouyang, and W. Y. Ching, Acta Mater. **53**, 403 (2005).
[29] Y. Sato, T. Mizoguchi, F. Oba, M. Yodogawa, T. Yamamoto, and Y. Ikuhara, Appl. Phys. Lett. **84**, 5311 (2004).
[30] T. Mizoguchi, Y. Sato, J. P. Buban, K. Matsunaga, T. Yamamoto, and Y. Ikuhara, Appl. Phys. Lett. **87**, 241920 (2005).
[31] R. S. Mulliken, J. Am. Chem. Soc. **23**, 1823 (1955).
[32] S. D. Mo and W. Y. Ching, Phys. Rev. B **62**, 7901 (2000).
[33] T. Mizoguchi, I. Tanaka, S. Yoshioka, M. Kunisu, T. Yamamoto, and W. Y. Ching, Phys. Rev. B **70**, 045103 (2004).
[34] I. Tanaka, T. Mizoguchi, and T. Yamamoto, J. Am. Ceram. Soc. **88**, 2013 (2005).
[35] R. Hoffmann, Angew. Chem., Int. Ed. Engl. **26**, 846 (1987).
[36] M. Mizuno, I. Tanaka, and H. Adachi, Phys. Rev. B **59**, 15033 (1999).
[37] T. Mizoguchi, I. Tanaka, M. Yoshiya, F. Oba, K. Ogasawara, and H. Adachi, Phys. Rev. B **61**, 2180 (2000).
[38] T. Mizoguchi, K. Tatsumi, and I. Tanaka, Ultramicroscopy **106**, 1120 (2006).
[39] R. D. Leapman, P. L. Feyes, and J. Silcox, Phys. Rev. B **28**, 2361 (1983).
[40] M. Nelhiebel, P.-H. Louf, P. Schattschneider, P. Blaha, K. Schwarz, and B. Jouffrey, Phys. Rev. B **59**, 12807 (1999).
[41] C. Hébert-Souche, P. H. Louf, P. Blaha, M. Nelhiebel, J. Luitz, P. Schattschneider, K. Schwarz, and B. Jouffrey, Ultramicroscopy **83**, 9 (2000).
[42] P. Schattschneider, C. Hébert, H. Franco, and B. Jouffrey, Phys. Rev. B **72**, 045142 (2005).
[43] T. Mizoguchi, J. P. Buban, K. Matsunaga, T. Yamamoto, and Y. Ikuhara, Ultramicroscopy **106**, 92 (2006).
[44] G. Radtke, T. Epicier, P. Bayle-Guillemaud, and J. C. Le Bossé, J. Microsc. **210**, 60 (2003).
[45] R. F. Klie, H. Su, Y. Zhu, J. W. Davenport, J. C. Idrobo, N. D. Browning, and P. D. Nellist, Phys. Rev. B **67**, 144508 (2003).
[46] Y. S. Lee, Y. Murakami, D. Shindo, and T. Oikawa, Mater. Trans., JIM **41**, 555 (2000).